Article

Current Biology

Homology and the evolution of vocal folds in the novel avian voice box

Highlights

- Vocal tissues of the syrinx and larynx develop from different precursor tissues
- Syrinx vocal folds evolved via co-option of a developmental program from the larynx
- The common ancestor of crown birds likely had a syrinx with two sound sources

Authors

Charlie Longtine, Chad M. Eliason, Darcy Mishkind, ..., Evan P. Kingsley, Julia A. Clarke, Clifford J. Tabin

Correspondence

evan_kingsley@hms.harvard.edu (E.P.K.), julia_clarke@jsg.utexas.edu (J.A.C.), tabin@genetics.med.harvard.edu (C.J.T.)

In brief

Is the avian-specific vocal organ, the syrinx, in any way homologous to the larynx-based sound source of non-avian tetrapods? Longtine et al. show that, despite different embryonic source tissues, the vocal folds of the avian syrinx evolved by coopting a developmental genetic program from the vocal tissues of the non-avian larynx.

Longtine et al., 2024, Current Biology *34*, 1–12
February 5, 2024
https://doi.org/10.1016/j.cub.2023.12.013

CellPress

Please cite this article in press as: Longtine et al., Homology and the evolution of vocal folds in the novel avian voice box, Current Biology (2023), https://doi.org/10.1016/j.cub.2023.12.013

Current Biology

CellPress

Article

Homology and the evolution of vocal folds in the novel avian voice box

Charlie Longtine,[1] Chad M. Eliason,[2,5] Darcy Mishkind,[1] ChangHee Lee,[1] Michael Chiappone,[2] Franz Goller,[3,4] Jay Love,[3,6] Evan P. Kingsley,[1,*] Julia A. Clarke,[2,*] and Clifford J. Tabin[1,7,*]

[1]Department of Genetics, Harvard Medical School, Boston, MA 02115, USA
[2]The Jackson School of Geosciences and Department of Integrative Biology, The University of Texas at Austin, Austin, TX 78712, USA
[3]School of Biological Sciences, University of Utah, Salt Lake City, UT 84112, USA
[4]Department of Zoophysiology, University of Münster, 48149 Münster, Germany
[5]Present address: Negaunee Integrative Research Center, Field Museum of Natural History, Chicago, IL 60605, USA
[6]Present address: Department of Internal Medicine, University of Utah, Salt Lake City, UT 84132, USA
[7]Lead contact
*Correspondence: evan_kingsley@hms.harvard.edu (E.P.K.), julia_clarke@jsg.utexas.edu (J.A.C.), tabin@genetics.med.harvard.edu (C.J.T.)
https://doi.org/10.1016/j.cub.2023.12.013

SUMMARY

The origin of novel traits, those that are not direct modifications of a pre-existing ancestral structure, remains a fundamental problem in evolutionary biology. For example, little is known about the evolutionary and developmental origins of the novel avian vocal organ, the syrinx. Located at the tracheobronchial junction, the syrinx is responsible for avian vocalization, but it is unclear whether avian vocal folds are homologous to the laryngeal vocal folds in other tetrapods or convergently evolved. Here, we identify a core developmental program involved in avian vocal fold formation and infer the morphology of the syrinx of the ancestor of modern birds. We find that this ancestral syrinx had paired sound sources induced by a conserved developmental pathway and show that shifts in these signals correlate with syringeal diversification. We show that, despite being derived from different developmental tissues, vocal folds in the syrinx and larynx have similar tissue composition and are established through a strikingly similar developmental program, indicating that co-option of an ancestral developmental program facilitated the origin of vocal folds in the avian syrinx.

INTRODUCTION

Vocal folds (VFs) are known to share similar functional properties, vibratory regimes, and neuronal circuit cell types across disparate taxa, from frogs, to mice and humans, and to birds.[1–4] VFs in non-avian tetrapods are situated in the larynx, at the cranial end of the trachea, and are proposed to have been modified from an ancestral valve present in tetrapods capable of protecting the airway.[5,6] Self-sustained oscillations of VFs are driven by a myoelastic-aerodynamic mechanism dependent on the mechanical properties of the tissue, imparted largely by the extracellular matrix (ECM).[4] The vocal organ in birds, however, is situated lower in the airway, either close to the tracheobronchial junction (TBJ) or deep in the bronchi, where there are no known valves or valve-precursors in outgroup reptiles (Figures 1A and 7).[6,7] Little is known about the evolutionary and developmental origins of the avian syrinx and to what extent, if any, its structures are homologous to those of the larynx. In particular, it is unknown whether syringeal VFs are directly homologous (i.e., derived from the same developmental source and deploying the same developmental programs suggesting phylogenetic continuity), deeply homologous (i.e., derived from a novel embryonic tissue but re-deploying ancestral developmental programs), or have a completely novel evolutionary origin of VFs (i.e., derived from novel embryonic tissues and induced via novel regulatory mechanisms).

The morphology of the syrinx in the most recent common ancestor of living birds is ambiguous.[6,7] In extant birds, the syrinx shows remarkably diverse morphology, positioning, and number of sound sources.[6–12] Two important functional classes of syrinxes are those that produce sound using a single pair of vibratory membranes in the lower trachea, such as in tinamous, pigeons, and parrots, and those that produce sound using two pairs of vibratory tissue located at or below the TBJ, such as in songbirds, penguins, and ducks.[4,8,9,11–13] Paired sound sources can allow complex vocalization, including simultaneous production of two fundamental frequencies and rapid switching between sources.[13–16] The extreme diversity of this organ and lack of molecular markers for avian VFs have made it difficult to infer the ancestral syringeal morphology, particularly the presence of a single sound source or paired sound sources.[6,7]

RESULTS

To investigate the evolutionary origin of the syrinx, we began by characterizing embryonic development of this organ in chicken (*Gallus domesticus*), which forms functional VFs prior to hatching.[17] Syringeal cartilage first differentiates in the chicken syrinx at Hamilton-Hamburger (HH) stage 35,[18] and VF primordia are first visible between the two enlarged syringeal cartilage elements around HH37 and HH38 (Figure 1B). We found that the ECM begins to be enriched in the VFs starting around HH37

Please cite this article in press as: Longtine et al., Homology and the evolution of vocal folds in the novel avian voice box, Current Biology (2023), https://doi.org/10.1016/j.cub.2023.12.013

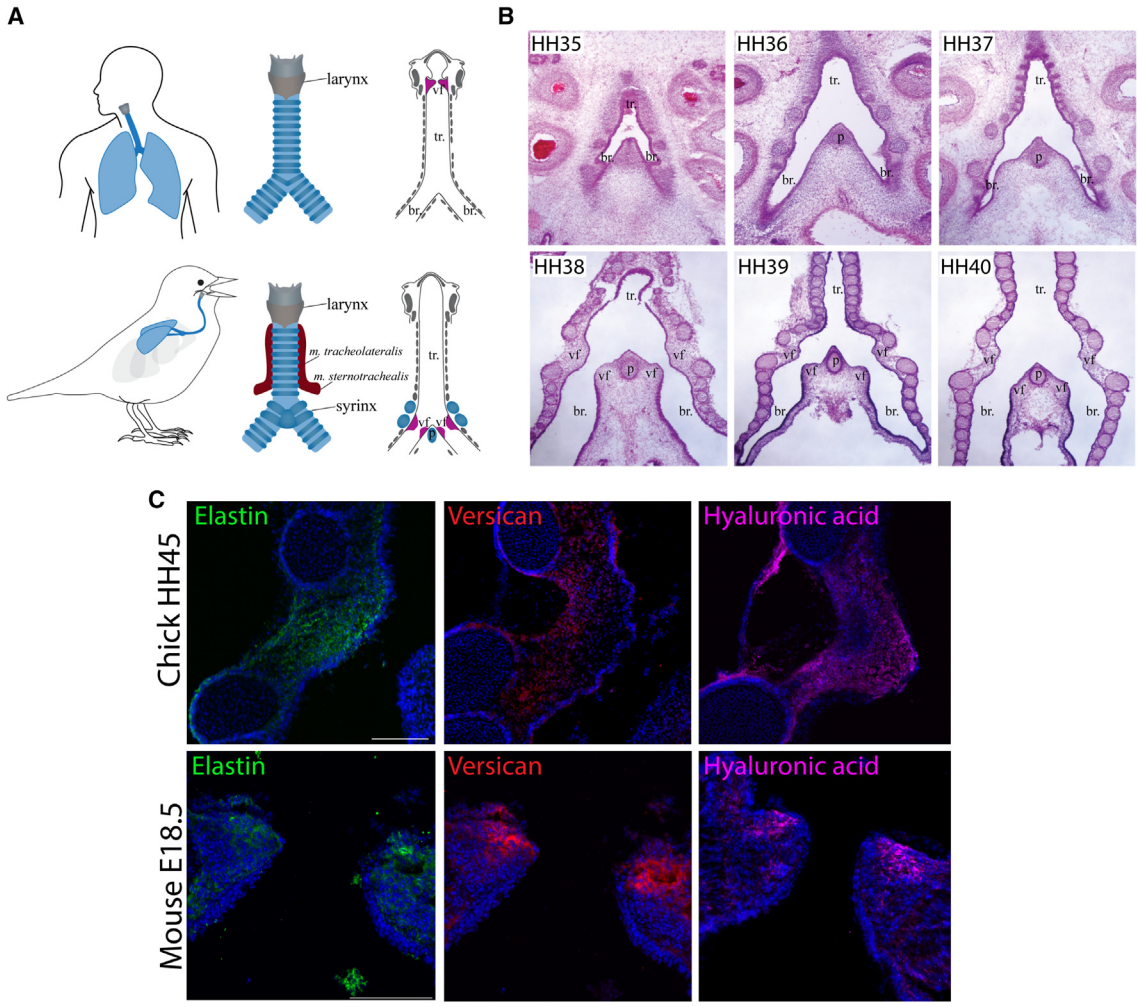

Figure 1. Developmental characterization of avian vocal folds

(A) Schematic of laryngeal and syringeal morphology. Novel extrinsic musculature (*M. tracheolateralis* and *M. sternotrachealis*, red) and enlarged tracheobronchial cartilage elements (dark blue) are illustrated in the frontal view (center). The shift in position of the vocal folds (magenta) from the larynx to syrinx in avians is illustrated in the cross-sectional view (right).

(B) H&E staining of coronal sections of the developing chick syrinx. At HH37, the vocal fold primordia are first visible at the TBJ between the two enlarged syringeal cartilage elements and continue to expand from HH38 to HH40.

(C) Immunofluorescence of extracellular matrix components elastin (green), versican (red), and hyaluronic acid (magenta) with DAPI (blue) in HH45 chick vocal folds and E18.5 mouse vocal folds. Scale bars, 100 μm. DAPI, 4′,6-diaminidino-2-phenylindole. tr, trachea; br, bronchi; vf, vocal fold; p, pessulus.

See also Figure S1.

and increases until hatching (Figures S1A and S1B). We screened for a variety of ECM molecules known to be present in different connective tissues and found that elastin, versican, and hyaluronic acid (HA) are all highly upregulated in chick embryonic VFs compared with the surrounding mesenchyme (Figures 1C, S1A, and S1D). When HA is digested using hyaluronidase, VF area decreases and cells become more densely packed (Figures S1B, S1E, and S1F), suggesting a role for HA in the expansion of VF tissue, similar to the role for HA in the expansion of the gut mesentery during chick development.[19]

To identify regulatory pathways involved in chick VF development, we performed spatially barcoded RNA sequencing (RNA-seq) of HH39 chick VFs, tracheal mesenchyme, and tracheal cartilage using Light-seq[20] (Figures 2A, 2B, and S1H). Following hierarchical clustering to separate samples by tissue type (Figure 2A), we identified a set of genes upregulated in VFs (Figures 2A and 2B). A subset of these were validated using immunofluorescence (IF), including thyroid hormone receptor A (*THRA*), *PDGFRA*, *SOX9*, *SERPINH1*, *PTER*, *OTX2*, and *TBX20* (Figure 2D). Others were validated by whole-mount *in situ* hybridization, including retinoic acid (RA) receptor responder 1 (*RARRES1*) and the RA synthesis gene *ALDH1A2*. Both *ALDH1A2* and *RARRES1* were expressed in the lateral mesenchyme, adjacent to the nascent VF at HH37 and HH39. Conversely, *CYP26C1*, which encodes an RA catabolizing enzyme, was expressed throughout the tracheal and bronchial mesenchyme but excluded from the VF anlagen (Figure 2C). This suggests the presence of localized RA signaling in the

Please cite this article in press as: Longtine et al., Homology and the evolution of vocal folds in the novel avian voice box, Current Biology (2023), https://doi.org/10.1016/j.cub.2023.12.013

CellPress

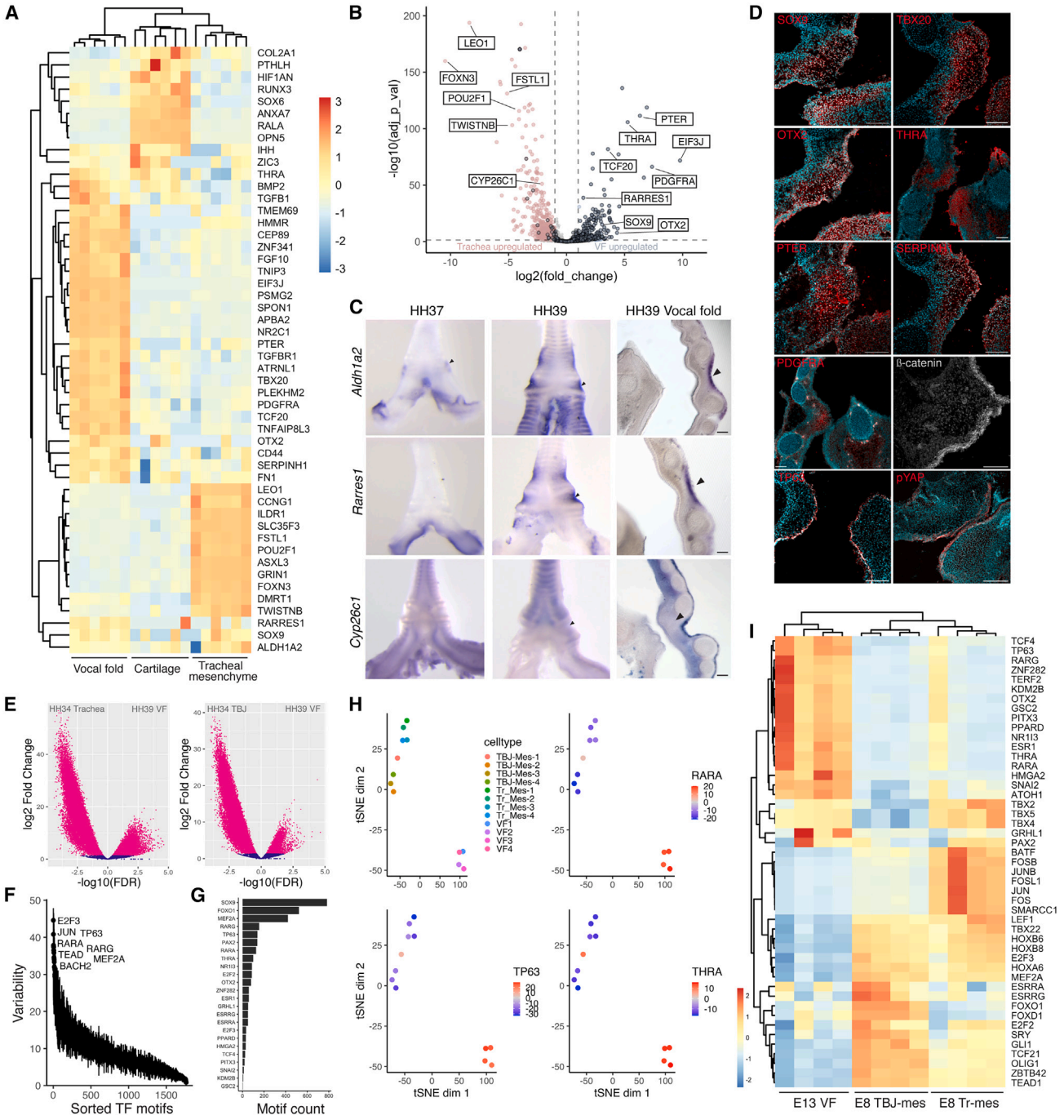

Figure 2. Gene expression and chromatin accessibility in the developing chick vocal folds

(A) Heatmap of Light-seq gene expression data from HH39 chick vocal folds, airway cartilage, and tracheal mesenchyme.

(B) Volcano plot showing differentially expressed genes in HH39 vocal fold (blue) versus tracheal mesenchyme (pink). Genes that are also significantly differentially expressed in vocal fold versus cartilage are points outlined in black.

(C) Whole-mount *in situ* hybridizations for retinoic acid signaling pathway genes in HH37 and HH39 syrinxes. Arrows indicate nascent vocal folds.

(D) Immunofluorescence for differentially expressed genes in HH39 vocal fold and TFs that show differential motif accessibility in vocal fold ATAC-seq. Scale bars, 100 μm.

(E) Differential accessibility of chromatin peaks in HH39 vocal fold compared with HH34 tracheal mesenchyme and HH34 TBJ.

(F) Plot of chromVAR chromatin variability scores for all TF-binding motifs assayed across all tissue types.

(G) Total TF-binding motif count in differentially accessible ATAC-seq peaks in which the nearest gene is significantly upregulated in HH39 vocal fold RNA-seq data.

(legend continued on next page)

Please cite this article in press as: Longtine et al., Homology and the evolution of vocal folds in the novel avian voice box, Current Biology (2023), https://doi.org/10.1016/j.cub.2023.12.013

developing chick VFs. Together, these results provide a set of candidate genes and pathways that may be involved in syrinx VF morphogenesis.

To further investigate the key genes regulating chick VF development, we performed assays for transposase-accessible chromatin with sequencing (ATAC-seq)[21] on manually dissected HH39 VFs compared with HH34 tracheal mesenchyme and TBJ mesenchyme. We identified 60,320 peaks significantly differentially accessible between VFs and tracheal mesenchyme and 58,157 peaks different between VFs and TBJ mesenchyme (Figure 2E). We next examined whether there were specific transcription factor (TF) binding motifs specifically associated with chromatin accessibility in HH39 VFs. Using chromVAR,[22] we identified matches to known TF-binding sites in the chick genome and calculated a bias-corrected genome-wide chromatin variability score for TF-binding motifs (Figures 2F–2I, S2A, and S2B). Among the most highly variable motifs that become more accessible during VF differentiation are motifs of RA receptors RARA/G, Wnt signaling effector TCF4, TP63/p63, OTX2, and THRA (Figures 2H and 2I). The presence of nuclear β-catenin in HH39 VF mesenchyme and TP63 in the VF epithelium (Figures 2D and S3A) further supports activation of Wnt signaling and TP63 during VF differentiation. To identify which TFs may be driving VF-specific gene expression, we quantified the total number of TF-binding motifs present in VF-specific ATAC peaks whose nearest gene is upregulated in the VF (Figure 2G). Among the top motifs in these peaks were SOX9, THRA, TP63, OTX2, RARA/G, and FOXO1, which are downstream of PDGFRα signaling.[23] Using TF-binding site accessibility and gene expression mutual information, we inferred putative tissue-specific gene regulatory networks in the trachea and VFs (Figures S2C–S2J). To infer key nodes in these networks, we used eigenvector centrality, a weighted degree vector that depends on the centrality of its neighbors, and identified FOXO1, SOX9, TP63, ESRRG, PPARD, THRA, and RARA as the top scoring TFs in the VF network (Figure S2I). We thus reasoned that these TFs may be regulators of VF-specific gene expression.

To test the functional role of thyroid hormone and RA signaling in the differentiation of chick VFs, we used a small-molecule pan-RAR inhibitor[24] (AGN193109) and THRA inhibitor (NH-3) to repress RA and thyroid hormone signaling *in ovo* from HH38 to HH45 (Figures 3A and S3B). Treated VFs had significantly lower levels of SOX9, HA, THRA, and PDGFRα (Figures 3A and 3B) and also showed a VF-specific decrease in proliferation and were smaller than control VFs (Figures S3E, S3F, and S3I). To determine whether RA is sufficient to induce differentiation of airway mesenchyme into VF tissue, we treated HH37 tracheas with RA at different concentrations in explant culture for 6 days (Figures 3 and S3H). RA treatment resulted in slightly increased HA deposition in the tracheal mesenchyme but was not sufficient to induce SOX9 in the non-cartilage mesenchyme. RA is thus required for specification of chick VFs but is not sufficient to fully induce VF differentiation in tracheal mesenchyme. To test whether SOX9 is upstream of ECM deposition in VFs, we infected cultured chick embryonic tracheal cells with a SOX9-expressing RCAS virus and observed an increase in HA, elastin, and versican deposition compared with a control virus (Figures 3C, 3E, and S3C). Conversely, overexpression of dominant-negative SOX9[25] (dnSOX9) in cultured VF cells led to a decrease in VF ECM (Figures 3D and 3F). THRA and RA thus play a role in the induction of VF-specific genes, including SOX9, while SOX9 itself is involved in the deposition of VF ECMs. Other upstream factors likely cooperate with THRA and RA signaling to induce SOX9, either directly or indirectly.

To investigate variation in this signaling pathway and its likely ancestral condition in Aves, we examined the expression of SOX9, PDGFRα, and *ALDH1A2* in Palaeognathae, the sister taxon to all other extant birds. In the ostrich, *ALDH1A2* is expressed in the syringeal mesenchyme at stage 39 prior to VF expansion (Figures S4A and S4B) and remains upregulated in the VF at later stages, along with SOX9 (Figures 4B and S4B). Similarly, the emu and rhea also express SOX9, PDGFRα, and *ALDH1A2* in late-embryonic VFs (Figures 4C, 4D, and S4C). The shared expression of these genes in the VFs of both Palaeognathae and an additional Galloanserae (duck; Figure S4D) suggests that this signaling axis dates back to the common ancestor of all living birds and possibly to the origin of syringeal VFs.

Expression patterns of SOX9, PDGFRα, and *ALDH1A2* in late-stage male and female ostrich embryos, as well as the morphology of pre- and post-hatch specimens, suggest the presence of two sound sources that persist in juveniles (Figures 4B and 5). Observation of a single sound source in an excised adult ostrich syrinx in a prior physiological study[4] suggests that the ostrich phonatory regime may shift during post-hatch development. Gene expression patterns in late-stage embryos of emu and rhea similarly show embryonic specification of two pairs of VFs (Figures 4B–4D). Although the number of sound sources present in chicken has been ambiguous in the literature,[17,26] our molecular markers show clear evidence of the formation of paired sound sources (Figures 1B and 2D) in the embryos that persist into post-hatch stages (Figure 5). Endoscopy of a vocalizing chicken hatchling functionally confirms *in vivo* function of two paired sound sources and not a single sound source in the trachea, as suggested previously[17,26] (Figure S7H; Video S1).

Phylogenetic analyses recover high support (maximum likelihood estimate of probability of paired sound sources at root = 0.99) for two sound sources in the common ancestor of crown birds (Figures 4A and S5A–S5C), despite ambiguity in the number of sound sources in adult ostrich. This support is also robust to uncertainty in taxon selection and phylogeny (Figure S5C; STAR Methods). Together, these allow robust inference of embryonic specification of paired sound sources in the common ancestor of Aves and the repeated shift to single sound sources in multiple taxa, including tinamous,[4] pigeons and doves,[9] and parrots (Figures 4A and S5A–S5C). To further understand the suite of morphological structures that may have been present

(H) T-distributed stochastic neighbor embedding (t-SNE) plot showing groupings of each tissue type based on TF-binding motif accessibility in the consensus peak set (top left). TF-binding motif accessibility for individual TFs (RARA, TP63, and THRA) are plotted on the t-SNE reduction.
(I) Heatmap of chromVAR TF motif deviations for highly variable motifs in each sample type.
See also Figures S1, S2, and S4.

Please cite this article in press as: Longtine et al., Homology and the evolution of vocal folds in the novel avian voice box, Current Biology (2023), https://doi.org/10.1016/j.cub.2023.12.013

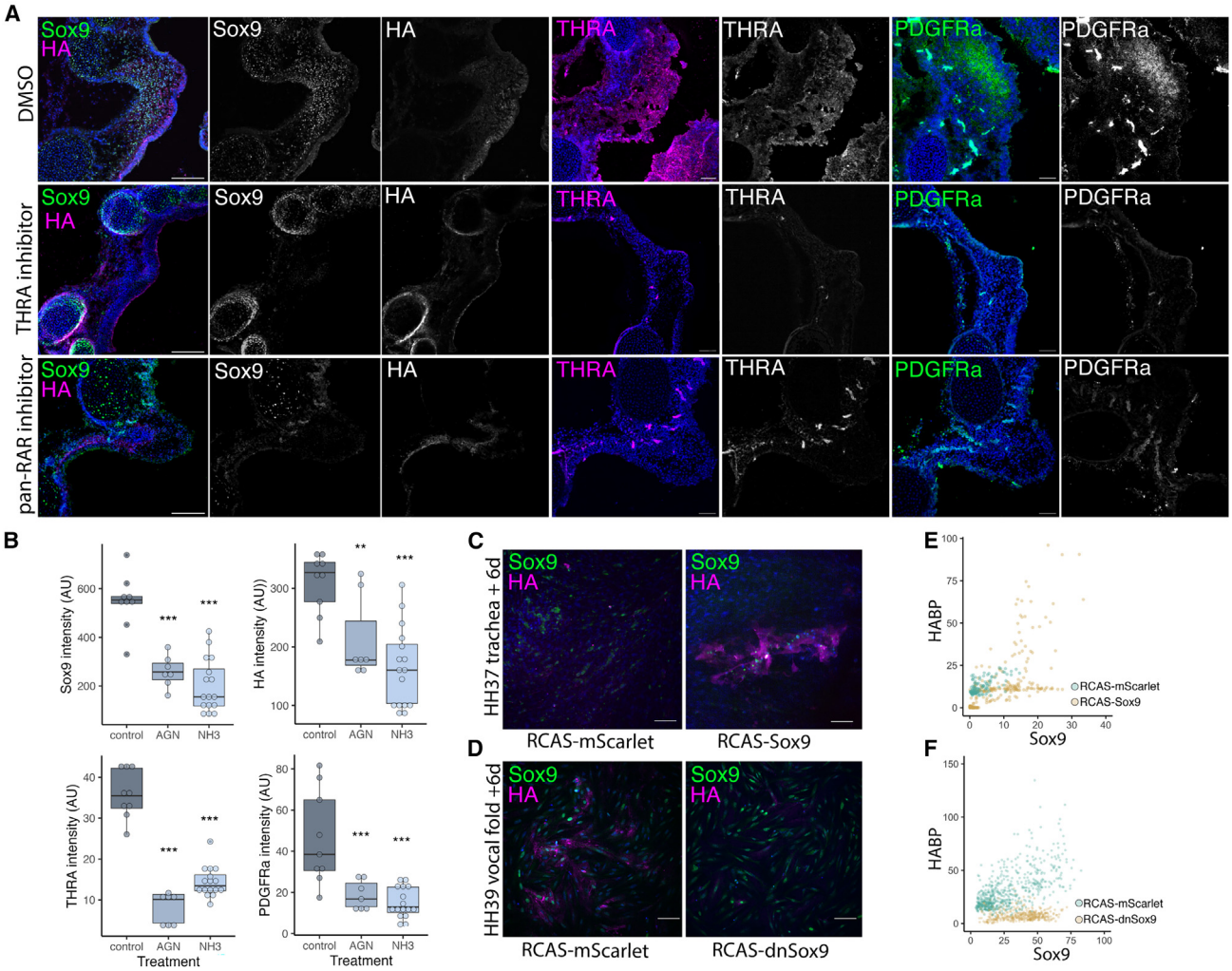

Figure 3. Retinoic acid and Sox9 are required for proper vocal fold specification

(A) Immunofluorescence of SOX9, hyaluronic acid (HA), THRA, and PDGFRa in HH45 vocal folds treated at HH38 with either DMSO, pan-RAR inhibitor (AGN193109), or THRA inhibitor (NH-3). Scale bars, 100 μm.

(B) Quantification of vocal fold SOX9, HA, THRA, and PDGFRa fluorescence intensity from (A). *p < 0.05, **p < 0.01, ***p < 0.001. Boxes indicate first quartile, median, and third quartile; whiskers show range.

(C) SOX9 and HA immunofluorescence in HH37 chick tracheal cells cultured for 6 days treated with RCAS-mScarlet or RCAS-Sox9.

(D) HH39 chick vocal fold cells treated with RCAS-mScarlet or RCAS-dnSox9 for 6 days. Scale bars, 100 μm.

(E and F) Quantification of HA and SOX9 intensity in (E) control- versus SOX9- or (F) control- versus dnSox9-treated cell cultures.

See also Figure S3.

in the syrinx in the common ancestor of Aves, we also performed ancestral state reconstructions for the presence of the pessulus—the midline cartilage element at the TBJ with debated functional significance[6,7] but which has been proposed to support paired sound sources in some birds and was previously suggested to be a derived trait of Neognathae[7]—and for the presence of intrinsic syringeal muscles. We infer the possible presence of a pessulus, but not intrinsic syringeal muscles, in the syrinx of the common ancestor of Aves (Figures S5D–S5G).

We find evidence that shifts in expression patterns of SOX9, PDGFRα, and *ALDH1A2* correlate with morphological diversification of the syrinx. In the emu, expansion of the expression domain of SOX9, PDGFRα, and *ALDH1A2* coincide with an anterior-posterior expansion of the VFs in the embryo, juvenile, and adult (Figures 4D and S5). We also examined expression of these markers in two taxa with highly derived syrinxes: budgerigars (Psittacidae) and penguins (Spheniscidae). The budgerigar syrinx is characterized by a single pair of VFs anterior to the TBJ. Paralleling this anterior shift in VFs, there is an anterior shift in the expression domains of SOX9, PDGFRα, and *ALDH1A2* (Figures 4F and S4E), suggesting that the evolution of a single sound source arises from an anterior shift in the specification of the lateral VFs into the trachea. Although penguins have two paired sound sources,[13] VFs on the lateral wall of the airway are reduced in size (Figure 4E) and vocalizations are presumably produced by vibration of the tympaniform membrane located on the medial walls of the bronchi.[27] In late-stage embryonic syrinxes from the gentoo penguin, which lack prominent lateral

Please cite this article in press as: Longtine et al., Homology and the evolution of vocal folds in the novel avian voice box, Current Biology (2023), https://doi.org/10.1016/j.cub.2023.12.013

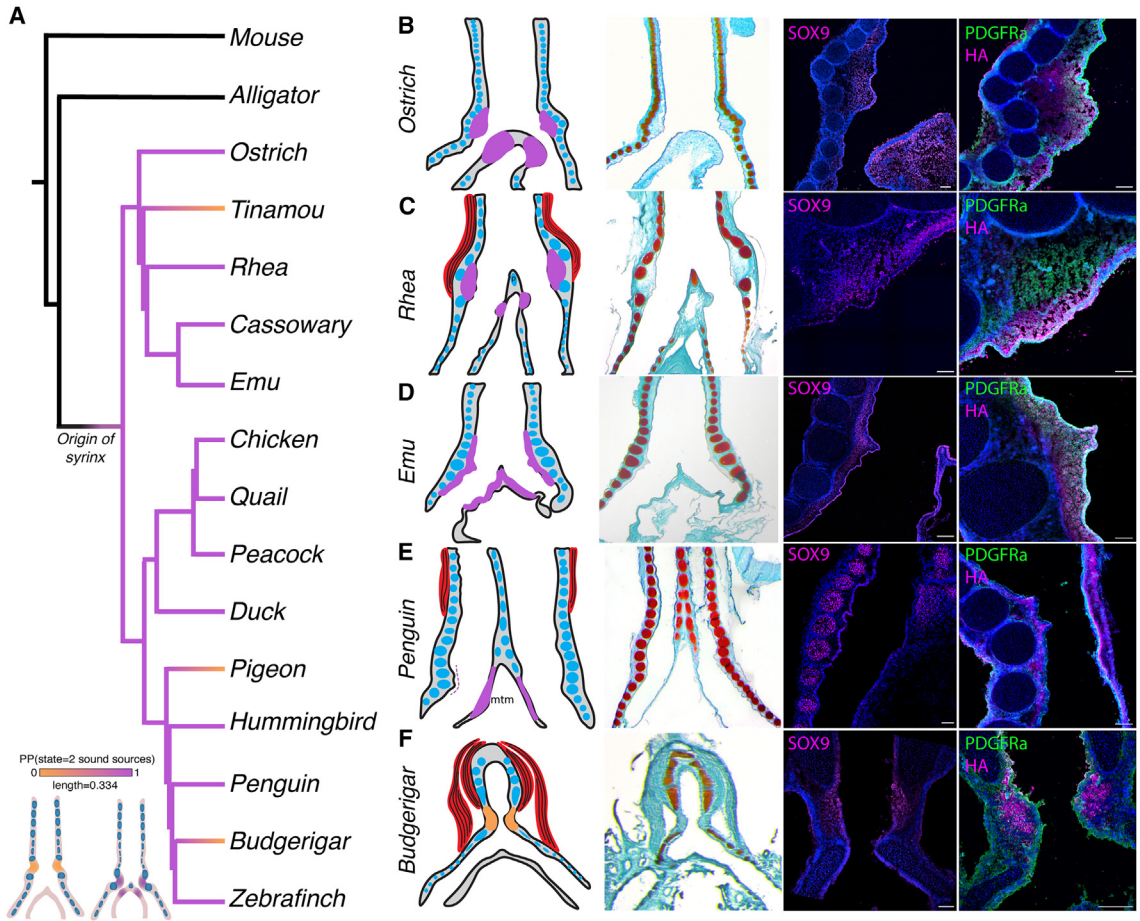

Figure 4. Vocal fold expression of SOX9 and PDGFRα are ancestral in Aves and shifts in gene expression correlate with diversification of syringeal vocal folds

(A) Ancestral state reconstruction of the number of sound sources in the avian lineage (see Figure S5).

(B–F) Schematic, safranin-O and fast green stain, and immunofluorescence for SOX9, PDGFRα, and hyaluronic acid (HA) in ostrich (HH41), rhea (HH41), emu (HH40), penguin (~HH38), and budgerigar (HH40) syrinxes. Vocal folds are indicated in purple (paired sound sources) or orange (single sound source), cartilage in blue, and syringeal musculature in red. Scale bars, 100 μm.

VFs in the embryo, we observed greatly reduced *ALDH1A2* and PDGFRα expression and no expression of SOX9 outside of cartilage condensations (Figures 4E and S4C), suggesting that reduced expression of the VF developmental program correlates with a reduction in VF size.

We next turned to the evolutionary relationship between syringeal VFs and the ancestral laryngeal VFs present in other tetrapods. Intriguingly, the entire suite of ECM factors we identified in the avian syrinx—elastin, versican, and HA—are similarly enriched in mammalian (Figure 1D) and crocodilian VFs.[28,29] Shared tissue composition and function in avian and mammalian VFs raises the possibility that VFs in the syrinx may be homologous to laryngeal VFs on a developmental level. Alternatively, syringeal VFs may have convergently evolved a similar ECM composition, driven by selection for mechanical properties consistent with their vibratory function.

The ECM-rich mesenchyme in mammalian VFs is derived from neural crest, while cranial mesenchyme forms the intrinsic vocalis muscle,[30] which has no correlate in the syrinx. Because neural crest is a migratory tissue during development, it was plausible that, in Aves, neural crest migrates to form VFs in a novel location. To test this hypothesis, we transplanted cranial or vagal neural crest from GFP-labeled donors into stage-matched wild-type chicks at HH8–HH11 (n = 42). At HH37, GFP-labeled neurons surround the airway and associated musculature, but neural-crest-derived tissue was not detected in the VF itself (Figures 6G, S6A, and S6B). We confirmed this result by electroporating a Piggybac transposon-based reporter *in ovo* into chick neural crest at HH8 (n = 21), HH9 (n = 16), HH10 (n = 13), and HH11 (n = 11) and observed no neural crest cells contributing to SOX9-positive VF cells (Figures 6I and S6C). In contrast, we fate-mapped lateral plate mesoderm, which is known to contribute to chick trachea and bronchi,[31] by injecting lentivirus-GFP into the coelom at HH11 (Figures 6J, S6D, and S6E). GFP-labeled lateral plate mesoderm co-localized with SOX9-positive VF cells, suggesting that the VFs in chick are derived not from neural crest as in the mammalian larynx, but instead primarily from lateral plate mesoderm. The VFs in the chick syrinx and mouse larynx derive from two distinct embryonic tissues, suggesting they are not

Please cite this article in press as: Longtine et al., Homology and the evolution of vocal folds in the novel avian voice box, Current Biology (2023), https://doi.org/10.1016/j.cub.2023.12.013

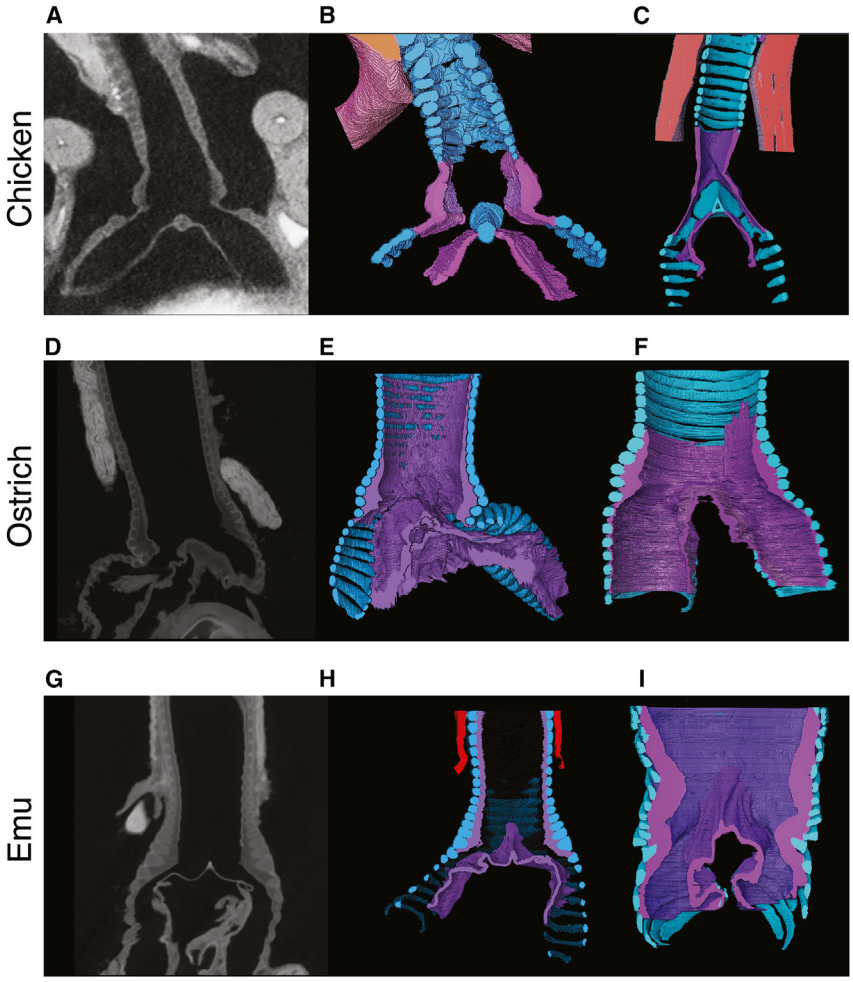

Figure 5. Paired sound sources in ostrich, emu, and chicken persist into juvenile and adult birds

(A) Iodine-enhanced contrast X-ray computed tomography (CT) data from the syrinx from a 2-day-old domestic chicken.

(B) Cut-through of a volumetric rendering of the 2-day-old domestic chicken syrinx in (A).

(C) Cut-through of a volumetric rendering of adult domestic chicken syrinx.

(D) Iodine-enhanced contrast CT data from 2-day-old ostrich syrinx.

(E) Cut-through of a volumetric rendering of the 2-day-old ostrich syrinx in (D).

(F) Cut-through of a volumetric rendering of a 14-day-old ostrich syrinx.

(G) Iodine-enhanced contrast CT data of the syrinx from a juvenile emu.

(H) Cut-through of a volumetric rendering of the juvenile emu syrinx in (G).

(I) Cut-through of a volumetric rendering from CT imaging of an adult emu syrinx.

homologous structures and that the syrinx is therefore an evolutionary novel organ.

Despite their distinct developmental origins, we speculated that shared developmental processes may underlie laryngeal and syringeal VF formation. Evolutionary novelties have repeatedly been shown to be derived from existing developmental programs.[32–35] When such programs are co-opted from an analogous morphological structure, the structures can be said to share deep homology.[33]

To determine whether syringeal VFs evolved via a novel VF developmental program or co-opted an existing laryngeal VF program, we performed Light-seq on embryonic day (E)18.5 mouse VFs, cartilage, and tracheal mesenchyme (Figures 6A, 6B, and S1G). We identified clusters of genes that are chick-VF-specific, mouse-VF-specific, and upregulated in both species (Figure 6F). Although RA pathway genes were not upregulated at this stage (Figure 6B), a number of key TFs and developmental genes present in the chick VFs were also upregulated in the mouse at E18.5, including SOX9, TBX20, OTX2, THRA, and PDGFRα (Figures 6C and 6F). We also observed nuclear β-catenin (Figure 6C), which has previously been implicated in the establishment of VF progenitor cells at early stages of laryngeal development.[36] SOX9, THRA, and PDGFRα expression in the VF is maintained in the adult mouse (Figure 6E), and SOX9 is expressed in late-embryonic macaque VFs (Figure 6H). Although *ALDH1A3* and SOX9 are also present in the VFs of alligators (Figure S7A), a member of the crocodilians, which are the closest extant relatives of birds, neither *ALDH1A2/3* nor SOX9 were expressed in the alligator or mouse TBJ nor in the mesenchyme of the avian larynx (Figures S7A–S7C), further indicating that their activities correlate with the presence of VFs, not anatomical location. The finding that SOX9 is expressed in the developing mouse VFs provided the opportunity to functionally test whether SOX9 acts upstream of ECM production in the mammalian airway as it does in the chick (Figures 3C–3F). Overexpression of SOX9 in cultured E16.5 mouse non-cartilage tracheal mesenchyme induced an upregulation of HA, elastin, and versican, suggesting that existing competency to this program in non-cartilage airway mesenchyme may have facilitated the evolution of syringeal VFs (Figures 6D, S7F, and S7G). In addition, this is consistent with a similar role for SOX9 in the developing laryngeal VFs.

The mouse VF is characterized not only by an ECM-rich mesenchyme but also a specialized epithelium overlying this tissue. The epithelium of the developing mouse VFs is marked by degradation of the basement membrane and loss of epithelial cell polarity (Figure S7E), correlated with upregulation of TP63 and phosphorylated YAP.[37,38] In the chick VFs, we identified a strikingly similar modification of the basement membrane structure and cell polarity in the epithelium overlying the developing chick focal folds (Figures S7D and S7E). Moreover, as these epithelial changes occur, TP63 and phosphorylated YAP are strongly detected in the syrinx epithelium (Figures 2D, S3A, and S3B), concurrent with increased accessibility of TP63 binding site motifs in VF chromatin (Figure 2H). In addition, both THRA and RA pathway inhibition *in ovo* attenuates localized YAP phosphorylation in the developing chick VF (Figures S3B

Please cite this article in press as: Longtine et al., Homology and the evolution of vocal folds in the novel avian voice box, Current Biology (2023), https://doi.org/10.1016/j.cub.2023.12.013

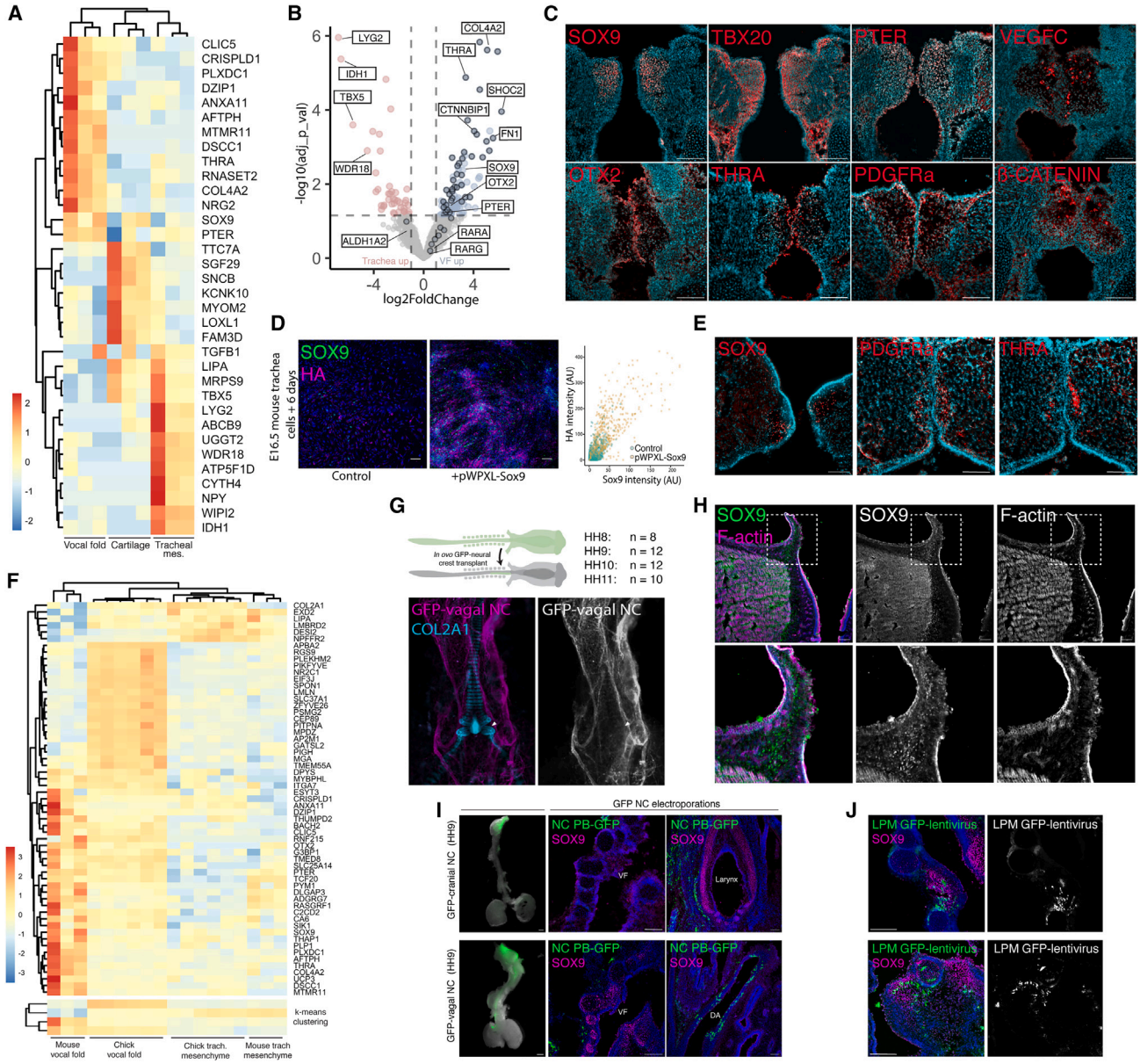

Figure 6. Co-option of laryngeal developmental program in the avian syrinx into lateral plate mesoderm

(A) Heatmap of Light-seq gene expression data from E18.5 mouse vocal folds, laryngeal cartilage, and tracheal mesenchyme.

(B) Volcano plot showing differentially expressed genes in E18.5 vocal fold (blue) versus tracheal mesenchyme (pink). Genes that are also significantly differentially expressed in vocal fold versus cartilage are points outlined in black.

(C) Immunofluorescence (IF) for genes upregulated in E18.5 mouse vocal folds, which are also upregulated in developing chick vocal folds. Scale bars, 100 μm.

(D) Immunofluorescence for SOX9 (green) and HA (magenta) in E16.5 mouse tracheal cells cultured for 6 days after transfection with mScarlet or pWPXL-Sox9. Scale bars, 100 μm. Right panel shows quantification of SOX9 and HA in control and treated tracheal cell cultures.

(E) IF for embryonic vocal fold marker genes in adult mouse vocal folds. Scale bars, 200 μm.

(F) Heatmap of RNA-seq data from HH39 chick airways and E18.5 mouse airways showing shared and distinct gene expression programs in chick and mouse vocal folds.

(G) Schematic of transplants of neural crest tissue from GFP chicks into wild-type chicks from HH8 to HH11 and whole-mount IF for COL2A1 in airways from chicks with GFP-neural crest transplants. Arrowhead indicates vocal fold.

(H) IF for SOX9 and F-actin in late-embryonic macaque vocal fold. Scale bars, 100 μm.

(I) Whole-mount images of HH39 chick airways transplanted cranial or vagal neural crest at HH9 (left). Piggybac-GFP-labeled neural crest cells (right) do not migrate into syringeal vocal folds but are present in the larynx and dorsal aorta (DA). Scale bars, 100 μm.

(J) Lentivirus-GFP injected into HH11 chick lateral plate mesoderm contributes to SOX9-positive cells in both lateral (top) and medial (bottom) vocal folds at HH39. Scale bars, 100 μm.

See also Figures S6 and S7.

Please cite this article in press as: Longtine et al., Homology and the evolution of vocal folds in the novel avian voice box, Current Biology (2023), https://doi.org/10.1016/j.cub.2023.12.013

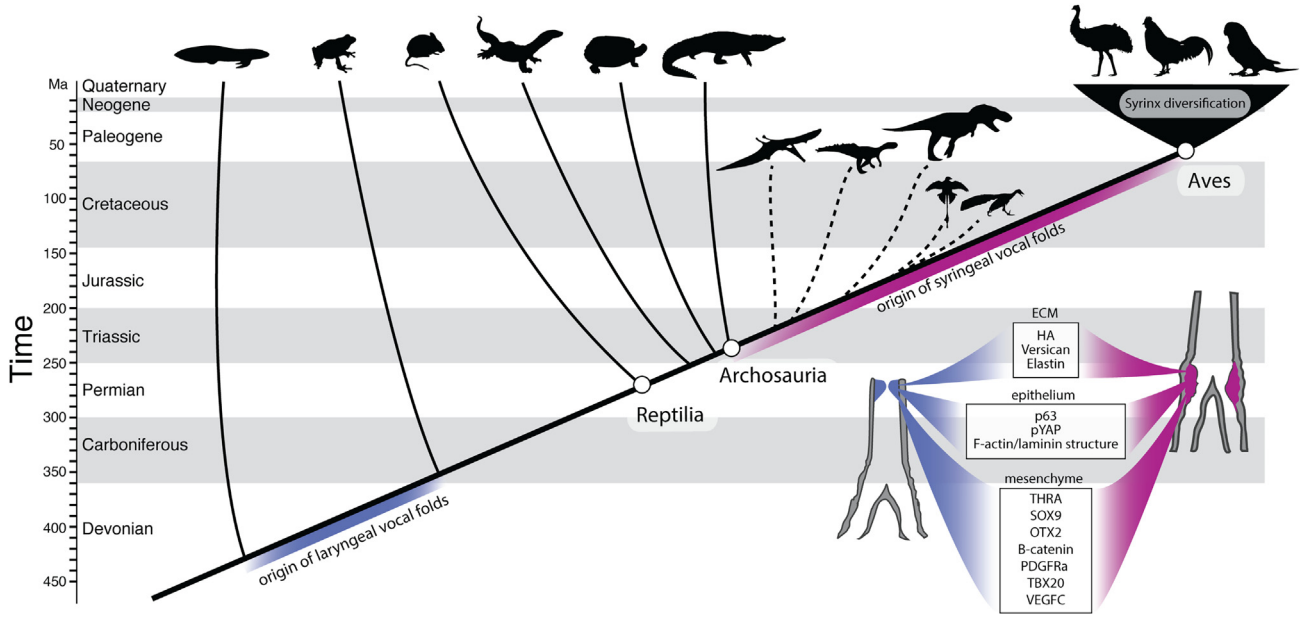

Figure 7. Schematic summarizing the results of this study

The cladogram highlights the evolution of laryngeal vocal folds before the origin of tetrapods (blue) and the syrinx (purple) prior to the origin of Aves. The lower right shows the molecular components that are shared between laryngeal vocal folds in non-birds and syringeal vocal folds in birds. Changes in expression of these components correlates with evolution of syrinx morphology within Aves (upper right).

and S3E), suggesting cross-tissue regulation coordinating epithelial and mesenchymal VF programs.

DISCUSSION

Taken together, the shared expression in both the laryngeal and syringeal VFs of a mesenchymal gene regulatory network, consisting in part of THRA, SOX9, PDGFRa, TBX20, β-catenin, and OTX2 (Figures 1D and 6C), combined with similar epithelial processes, including TP63, phosphorylated YAP, and a unique epithelial laminin and F-actin structure (Figures 2, S3A, S3B, S7D, and S7E), suggest that the developmental program for VFs in the syrinx was, at least in part, co-opted from the ancestral laryngeal program into the lateral plate mesoderm-derived lower airway, and there is thus deep homology between these two vibratory tissues (Figure 7). Notably, there are a number of genes and pathways that are present in the chick VFs that are not detected in those of the mouse. One such example is the RA pathway, although evidence for RA signaling is seen in the developing laryngeal VFs of the alligator, suggesting that RA signaling may have been part of the regulatory network of the laryngeal VFs in the archosaurian ancestor that first evolved a syrinx. The absence in the mouse larynx of other genes active in the developing chick syrinx may be a result of timing differences between species; transcriptional profiling of mouse VFs at additional stages may reveal further commonalities with the chick. Alternatively, some chick-specific VF genes likely represent novel, lineage-specific aspects of avian VF development not present in the larynx. Although a core gene regulatory module from the laryngeal VFs appears to be redeployed in the VFs of the syrinx, expression of novel modules may be required to induce the VF program at the TBJ from a different precursor tissue, or to produce syrinx-specific tissue properties. The interconnected VF regulatory module of TFs and signaling molecules can also be interpreted as constituting a character identity network (ChIN), as defined by Wagner et al.[34,39,40] The VFs in the syrinx and larynx are distinct tissues and not composed of identical or homologous cell types. However, our data suggest that a core gene regulatory module involved in the development of avian VFs is derived from an ancestral gene regulatory module shared with mammalian VFs.

VFs in the larynx of early tetrapods have been assumed to have evolved from a valve-like structure.[5,6,41] RA is required for the formation of heart valve precursors[42,43] and SOX9 is required for the deposition of HA and other ECM in the developing endocardial cushions in both zebrafish[44] and mice.[45,46] An attractive hypothesis is thus that both laryngeal and syringeal VFs may have originated through re-deployment, at least in part, of an ancestral valve developmental program. It remains to be seen whether other examples of non-laryngeal VFs, such as the velar VFs in koalas[47] and nasal phonic lips used for echolocation in toothed whales,[48,49] evolved from a similar developmental mechanism. In sum, our results point to a deep homology between the syrinx and the larynx, where existing developmental processes from the larynx were redeployed in an avian ancestor at the TBJ, contributing to the development of VFs in a tissue of distinct developmental origin. The co-option in this ancestral tetrapod VF genetic program thus underlies a major morphological transition in dinosaurs, with shifts in this regulatory network generating the diversity of VF morphologies in living birds.

STAR★METHODS

Detailed methods are provided in the online version of this paper and include the following:

SUPPLEMENTAL INFORMATION

Supplemental information can be found online at https://doi.org/10.1016/j.cub.2023.12.013.

ACKNOWLEDGMENTS

The authors wish to thank the Broad walk-up sequencing core (Broad Institute), the Microscopy Resources on the North Quad (MicRoN) core (Harvard Medical School), the Biopolymers Facility (Harvard Medical School) for providing experimental platforms used in this work, and M. Manceau and C. Curantz for assistance collecting penguin specimens. We thank M. Dyer and St. Jude DNB for their exceedingly generous support, enabling the efforts of E.P.K. We thank L. Legendre, K. Bader, M. Colbert, and H. Bilger for preparation and computed tomography (CT) imaging assistance and Z. Li and T. Riede for early discussion. pWPXL-SOX9 was a gift from B. Weinberg (Addgene plasmid # 36979), LiOn-CAG∞GFP was a gift from Jean Livet (Addgene plasmid # 154016), pCMV-hyPBase was a gift from Sanger Institute, GFP-lentivirus was a gift from C. Cepko and R. Delgado, and pmScarlet_C1 was a gift from D. Gadella (Addgene plasmid # 85042). Funding was provided by National Institutes of Health grant HD987234 (C.J.T.), Gordon and Betty Moore Foundation grant 4498 (J.A.C., F.G., and C.J.T.), and National Institutes of Health grant P51OD011092 (Oregon National Primate Research Center).

AUTHOR CONTRIBUTIONS

J.A.C., F.G., E.P.K., and C.J.T. conceived the study and obtained funding. C. Longtine, C.J.T., and E.P.K. designed the experiments. C. Longtine conducted RNA-seq and ATAC-seq experiments, electroporations, lentivirus injections, immunohistochemistry, *in situ* hybridization, cell culture, small-molecule perturbations, imaging, quantification, and sequencing analysis. C. Longtine and E.P.K. performed tissue grafts and histology. C. Longtine and C.M.E. did the ancestral state analyses. F.G. and J.L. performed airway endoscopy. M.C. and J.A.C. generated CT data and volumetric renderings. D.M. and C. Lee assisted with ATAC-seq. C. Longtine, E.P.K., and C.J.T. wrote the paper with input from all authors.

DECLARATION OF INTERESTS

The authors declare no competing interests.

Received: June 14, 2023
Revised: August 29, 2023
Accepted: December 6, 2023
Published: January 5, 2024

REFERENCES

1. Tecumseh Fitch, W. (2010). The Evolution of Language (Cambridge University Press).
2. Pfenning, A.R., Hara, E., Whitney, O., Rivas, M.V., Wang, R., Roulhac, P.L., Howard, J.T., Wirthlin, M., Lovell, P.V., Ganapathy, G., et al. (2014). Convergent transcriptional specializations in the brains of humans and song-learning birds. Science *346*, 1256846.
3. Colquitt, B.M., Merullo, D.P., Konopka, G., Roberts, T.F., and Brainard, M.S. (2021). Cellular transcriptomics reveals evolutionary identities of songbird vocal circuits. Science *371*, eabd9704.
4. Elemans, C.P.H., Rasmussen, J.H., Herbst, C.T., Düring, D.N., Zollinger, S.A., Brumm, H., Srivastava, K., Svane, N., Ding, M., Larsen, O.N., et al. (2015). Universal mechanisms of sound production and control in birds and mammals. Nat. Commun. *6*, 8978.
5. Negus, V.E. (1949). The Comparative Anatomy and Physiology of the Larynx (Hafner Publishing Company).
6. Kingsley, E.P., Eliason, C.M., Riede, T., Li, Z., Hiscock, T.W., Farnsworth, M., Thomson, S.L., Goller, F., Tabin, C.J., and Clarke, J.A. (2018). Identity and novelty in the avian syrinx. Proc. Natl. Acad. Sci. USA *115*, 10209–10217.
7. Clarke, J.A., Chatterjee, S., Li, Z., Riede, T., Agnolin, F., Goller, F., Isasi, M.P., Martinioni, D.R., Mussel, F.J., and Novas, F.E. (2016). Fossil evidence of the avian vocal organ from the Mesozoic. Nature *538*, 502–505.
8. King, A.S. (1989). Functional anatomy of the syrinx. In Form and Function in Birds, *4*, A.S. King, and J. McLelland, eds. (Academic Press).
9. Larsen, O.N.L., and Gollerf, F. (1999). Role of syringeal vibrations in bird vocalizations. Proc. R. Soc. Lond. B *266*, 1609–1615.
10. Goller, F., and Larsen, O.N. (1997). A new mechanism of sound generation in songbirds. Proc. Natl. Acad. Sci. USA *94*, 14787–14791.
11. Goller, F., and Larsen, O.N. (2002). New perspectives on mechanisms of sound generation in songbirds. J. Comp. Physiol. A Neuroethol. Sens. Neural Behav. Physiol. *188*, 841–850.
12. Ames, P.L. (1971). The morphology of the syrinx in passerine birds. Peabody Mus. Nat. His. Bull. *37*, 1–195.
13. Aubin, T., Jouventin, P., and Hildebrand, C. (2000). Penguins use the two-voice system to recognize each other. Proc. Biol. Sci. *267*, 1081–1087.
14. Miller, D.B. (1977). Two-voice phenomenon in birds: further evidence. Auk *94*, 567–572.
15. Suthers, R.A. (1990). Contributions to birdsong from the left and right sides of the intact syrinx. Nature *347*, 473–477.
16. Suthers, R.A. (1997). Peripheral control and lateralization of birdsong. J. Neurobiol. *33*, 632–652.
17. Gottlieb, G., and Vandenbergh, J.G. (1968). Ontogeny of vocalization in duck and chick embryos. J. Exp. Zool. *168*, 307–325.
18. Hamburger, V., and Hamilton, H.L. (1951). A series of normal stages in the development of the chick embryo. J. Morphol. *88*, 49–92.
19. Kurpios, N.A., Ibañes, M., Davis, N.M., Lui, W., Katz, T., Martin, J.F., Izpisúa Belmonte, J.C., and Tabin, C.J. (2008). The direction of gut looping is established by changes in the extracellular matrix and in cell:cell adhesion. Proc. Natl. Acad. Sci. USA *105*, 8499–8506.
20. Kishi, J.Y., Liu, N., West, E.R., Sheng, K., Jordanides, J.J., Serrata, M., Cepko, C.L., Saka, S.K., and Yin, P. (2022). Light-Seq: light-directed in situ barcoding of biomolecules in fixed cells and tissues for spatially indexed sequencing. Nat. Methods *19*, 1393–1402.
21. Corces, M.R., Trevino, A.E., Hamilton, E.G., Greenside, P.G., Sinnott-Armstrong, N.A., Vesuna, S., Satpathy, A.T., Rubin, A.J., Montine, K.S., Wu, B., et al. (2017). An improved ATAC-seq protocol reduces

background and enables interrogation of frozen tissues. Nat. Methods *14*, 959–962.

22. Schep, A.N., Wu, B., Buenrostro, J.D., and Greenleaf, W.J. (2017). chromVAR: inferring transcription-factor-associated accessibility from single-cell epigenomic data. Nat. Methods *14*, 975–978.
23. Xin, Z., Ma, Z., Hu, W., Jiang, S., Yang, Z., Li, T., Chen, F., Jia, G., and Yang, Y. (2018). FOXO1/3: potential suppressors of fibrosis. Ageing Res. Rev. *41*, 42–52.
24. Johnson, A.T., Klein, E.S., Gillett, S.J., Wang, L., Song, T.K., Pino, M.E., and Chandraratna, R.A. (1995). Synthesis and characterization of a highly potent and effective antagonist of retinoic acid receptors. J. Med. Chem. *38*, 4764–4767.
25. Lefebvre, V., Huang, W., Harley, V.R., Goodfellow, P.N., and de Crombrugghe, B. (1997). SOX9 is a potent activator of the chondrocyte-specific enhancer of the pro alpha1(II) collagen gene. Mol. Cell. Biol. *17*, 2336–2346.
26. Gross, W.B. (1964). Voice production by the chicken. Poult. Sci. *43*, 1005–1008.
27. Kriesell, H.J., Le Bohec, C., Cerwenka, A.F., Hertel, M., Robin, J.P., Ruthensteiner, B., Gahr, M., Aubin, T., and Düring, D.N. (2020). Vocal tract anatomy of king penguins: morphological traits of two-voiced sound production. Front. Zool. *17*, 5.
28. Riede, T., Li, Z., Tokuda, I.T., and Farmer, C.G. (2015). Functional morphology of the *Alligator mississippiensis* larynx with implications for vocal production. J. Exp. Biol. *218*, 991–998.
29. Lungova, V., and Thibeault, S.L. (2020). Mechanisms of larynx and vocal fold development and pathogenesis. Cell. Mol. Life Sci. *77*, 3781–3795.
30. Tabler, J.M., Rigney, M.M., Berman, G.J., Gopalakrishnan, S., Heude, E., Al-Lami, H.A., Yannakoudakis, B.Z., Fitch, R.D., Carter, C., Vokes, S., et al. (2017). Cilia-mediated Hedgehog signaling controls form and function in the mammalian larynx. eLife *6*, e19153.
31. Matsushita, S., and Matsushita, S. (1995). Fate mapping study of the splanchnopleural mesoderm of the 1.5-day-old chick embryo. Rouxs Arch. Dev. Biol. *204*, 392–399.
32. Averof, M., and Cohen, S.M. (1997). Evolutionary origin of insect wings from ancestral gills. Nature *385*, 627–630.
33. Shubin, N., Tabin, C., and Carroll, S. (2009). Deep homology and the origins of evolutionary novelty. Nature *457*, 818–823.
34. Wagner, G.P. (2014). Homology, Genes, and Evolutionary Innovation (Princeton University Press).
35. Hu, Y., Linz, D.M., and Moczek, A.P. (2019). Beetle horns evolved from wing serial homologs. Science *366*, 1004–1007.
36. Lungova, V., Verheyden, J.M., Sun, X., and Thibeault, S.L. (2018). β-catenin signaling is essential for mammalian larynx recanalization and the establishment of vocal fold progenitor cells. Development *145*, dev157677.
37. Lungova, V., Verheyden, J.M., Herriges, J., Sun, X., and Thibeault, S.L. (2015). Ontogeny of the mouse vocal fold epithelium. Dev. Biol. *399*, 263–282.
38. Mohad, V., Lungova, V., Verheyden, J., and Thibeault, S.L. (2021). Inactivation of Lats1 and Lats2 highlights the role of hippo pathway effector YAP in larynx and vocal fold epithelium morphogenesis. Dev. Biol. *473*, 33–49.
39. Wagner, G.P., and Lynch, V.J. (2010). Evolutionary novelties. Curr. Biol. *20*, R48–R52.
40. DiFrisco, J., Wagner, G.P., and Love, A.C. (2023). Reframing research on evolutionary novelty and co-option: character identity mechanisms versus deep homology. Semin. Cell Dev. Biol. *145*, 3–12.
41. Fitch, W.T., and Suthers, R.A. (2016). Vertebrate vocal production: an introductory overview. In Vertebrate Sound Production and Acoustic Communication, R.A. Suthers, W.T. Fitch, R.R. Fay, and A.N. Popper, eds. (Springer International Publishing), pp. 1–18.
42. El Robrini, N., Etchevers, H.C., Ryckebüsch, L., Faure, E., Eudes, N., Niederreither, K., Zaffran, S., and Bertrand, N. (2016). Cardiac outflow morphogenesis depends on effects of retinoic acid signaling on multiple cell lineages. Dev. Dyn. *245*, 388–401.
43. Li, J., Yue, Y., and Zhao, Q. (2016). Retinoic acid signaling is essential for valvulogenesis by affecting endocardial cushions formation in zebrafish embryos. Zebrafish *13*, 9–18.
44. Hofsteen, P., Plavicki, J., Johnson, S.D., Peterson, R.E., and Heideman, W. (2013). Sox9b is required for epicardium formation and plays a role in TCDD-induced heart malformation in zebrafish. Mol. Pharmacol. *84*, 353–360.
45. Akiyama, H., Chaboissier, M.-C., Behringer, R.R., Rowitch, D.H., Schedl, A., Epstein, J.A., and de Crombrugghe, B. (2004). Essential role of Sox9 in the pathway that controls formation of cardiac valves and septa. Proc. Natl. Acad. Sci. USA *101*, 6502–6507.
46. Lincoln, J., Kist, R., Scherer, G., and Yutzey, K.E. (2007). Sox9 is required for precursor cell expansion and extracellular matrix organization during mouse heart valve development. Dev. Biol. *305*, 120–132.
47. Charlton, B.D., Frey, R., McKinnon, A.J., Fritsch, G., Fitch, W.T., and Reby, D. (2013). Koalas use a novel vocal organ to produce unusually low-pitched mating calls. Curr. Biol. *23*, R1035–R1036.
48. Cranford, T.W., Amundin, M., and Norris, K.S. (1996). Functional morphology and homology in the odontocete nasal complex: implications for sound generation. J. Morphol. *228*, 223–285.
49. Reidenberg, J.S., and Laitman, J.T. (1988). Existence of vocal folds in the larynx of Odontoceti (toothed whales). Anat. Rec. *221*, 884–891.
50. McGrew, M.J., Sherman, A., Lillico, S.G., Ellard, F.M., Radcliffe, P.A., Gilhooley, H.J., Mitrophanous, K.A., Cambray, N., Wilson, V., and Sang, H. (2008). Localised axial progenitor cell populations in the avian tail bud are not committed to a posterior Hox identity. Development *135*, 2289–2299.
51. Serralbo, O., Salgado, D., Véron, N., Cooper, C., Dejardin, M.-J., Doran, T., Gros, J., and Marcelle, C. (2020). Transgenesis and web resources in quail. eLife *9*, e56312.
52. Nagai, H., Mak, S.S., Weng, W., Nakaya, Y., Ladher, R., and Sheng, G. (2011). Embryonic development of the emu, *Dromaius novaehollandiae*. Dev. Dyn. *240*, 162–175.
53. Murray, J.R., Varian-Ramos, C.W., Welch, Z.S., and Saha, M.S. (2013). Embryological staging of the Zebra Finch, *Taeniopygia guttata*. J. Morphol. *274*, 1090–1110.
54. Ferguson, M.W.J. (1985). Reproductive biology and embryology of the crocodilians. In Biology of the Reptilia, C. Gans, F. Billett, and P.F.A. Maderson, eds. (Wiley), pp. 329–491.
55. Ninomiya, Y., Zhao, W., and Saga, Y. (2016). GBIQ: a non-arbitrary, non-biased method for quantification of fluorescent images. Sci. Rep. *6*, 26454.
56. Pennell, M.W., Eastman, J.M., Slater, G.J., Brown, J.W., Uyeda, J.C., FitzJohn, R.G., Alfaro, M.E., and Harmon, L.J. (2014). geiger v2.0: an expanded suite of methods for fitting macroevolutionary models to phylogenetic trees. Bioinformatics *30*, 2216–2218.
57. Prum, R.O., Berv, J.S., Dornburg, A., Field, D.J., Townsend, J.P., Lemmon, E.M., and Lemmon, A.R. (2015). A comprehensive phylogeny of birds (Aves) using targeted next-generation DNA sequencing. Nature *526*, 569–573.
58. Kimball, R.T., Oliveros, C.H., Wang, N., White, N.D., Barker, F.K., Field, D.J., Ksepka, D.T., Chesser, R.T., Moyle, R.G., Braun, M.J., et al. (2019). A phylogenomic supertree of birds. Diversity *11*, 109.
59. Burleigh, J.G., Kimball, R.T., and Braun, E.L. (2015). Building the avian tree of life using a large-scale, sparse supermatrix. Mol. Phylogenet. Evol. *84*, 53–63.
60. Riede, T., Eliason, C.M., Miller, E.H., Goller, F., and Clarke, J.A. (2016). Coos, booms, and hoots: the evolution of closed-mouth vocal behavior in birds. Evolution *70*, 1734–1746.

61. Ronquist, F. (2004). Bayesian inference of character evolution. Trends Ecol. Evol. *19*, 475–481.

62. Revell, L.J. (2012). phytools: an R package for phylogenetic comparative biology (and other things). Methods Ecol. Evol. *3*, 217–223.

63. Forbes, W.A. (1881). On the conformation of the thoracic end of the trachea in the ratite birds. Proc. Zool. Soc. Lond. *49*, 778–788.

64. Yildiz, H., Bahadir, A., and Akkoç, A. (2003). A study on the morphological structure of syrinx in ostriches (*Struthio camelus*). Anat. Histol. Embryol. *32*, 187–191.

65. Logan, M., Pagán-Westphal, S.M., Smith, D.M., Paganessi, L., and Tabin, C.J. (1998). The transcription factor Pitx2 mediates situs-specific morphogenesis in response to left-right asymmetric signals. Cell *94*, 307–317.

66. Smith, T., Heger, A., and Sudbery, I. (2017). UMI-tools: modeling sequencing errors in unique molecular identifiers to improve quantification accuracy. Genome Res. *27*, 491–499.

67. Love, M.I., Huber, W., and Anders, S. (2014). Moderated estimation of fold change and dispersion for RNA-seq data with DESeq2. Genome Biol. *15*, 550.

Please cite this article in press as: Longtine et al., Homology and the evolution of vocal folds in the novel avian voice box, Current Biology (2023), https://doi.org/10.1016/j.cub.2023.12.013

STAR★METHODS

KEY RESOURCES TABLE

REAGENT or RESOURCE	SOURCE	IDENTIFIER
Antibodies		
SOX9	Millipore	Cat# AB5535; RRID:AB_2239761
phosphoH3S10	Millipore	Cat# 06-570; RRID:AB_310177
Biotinylated-HABP	EMD Millipore	Cat# 385911
Cleaved Caspase 3	Cell signaling	Cat# 9662; RRID:AB_331439
Laminin	Sigma-Aldrich	Cat# L9393; RRID:AB_477163
Versican	ThermoFisher	Cat# PA1-1748A; RRID:AB_2304324
Elastin	EMD Chemicals	Cat# MAB2503; RRID:AB_2099602
phosphoYAP	Cell signaling	Cat# 13008S; RRID:AB_2650553
THRA	ThermoFisher	Cat# PA1-211A; RRID:AB_325811
PDGFRa	R&D Systems	Cat# sc-338; RRID:AB_631064
SERPINH1	ThermoFisher	Cat# PA5-27832; RRID:AB_2545308
PTER	ThermoFisher	Cat# PA5-27801; RRID:AB_2545277
OTX2	ProteinTech	Cat# 13497-1-AP; RRID:AB_2157176
TBX20	Novus Biologics	MAB8124
VEGFC	ProteinTech	22601-1-AP
β-catenin	Millipore	05-665
Col2a1	DHSB	II-II6B3
Alexa Fluor 647 Phalloidin	Invitrogen	A22287
Bacterial and virus strains		
pWPXL-Sox9	Addgene	36979
LiOn-CAG∞GFP	Addgene	154016
pmScarlet_C1	Addgene	85042
Chemicals, peptides, and recombinant proteins		
Trypsin in EDTA	Sigma	T3924
DMEM	GIBCO	11960044
Pen/Strep	GIBCO	15240062
FBS	GIBCO	16000044
Proteinase K	NEB	P8107S
Blocking Reagent	Millipore-Sigma	11096176001
TSA Plus Cy3 and Fluorescein	Perkin-Elmer	NEL753001KT
OCT	VWR	25608-930
BM-Purple	Sigma-Aldrich	1442074001
Maxima H Minus Reverse Transcriptase (200 U/μL) (includes 5X buffer)	Thermo Scientific	FEREP0753
RNaseOUTTM Recombinant Ribonuclease Inhibitor	Invitrogen	10888019
TritonX-100	Sigma-Aldrich	T8787
Terminal Transferase	NEB	M0315
ddATP (100mM)	NEB	GE27-2051- 01
dNTP mix (10mM)	NEB	N04447
dATP	NEB	N04446
5M NaCl	Invitrogen	AM9760
Formamide (Deionized)	Invitrogen	AM9342

(*Continued on next page*)

Please cite this article in press as: Longtine et al., Homology and the evolution of vocal folds in the novel avian voice box, Current Biology (2023), https://doi.org/10.1016/j.cub.2023.12.013

Continued

REAGENT or RESOURCE	SOURCE	IDENTIFIER
Salmon-sperm DNA	ThermoFisher	AM9680
Dextran Sulfate (50%)	EMD	S4030
Bst DNA polymerase – large fragment	NEB	M0275
RnaseH	NEB	M0297
HiFi HotStart DNA polymerase, Kapa biosystems	Roche	KK2502
SYBR Green 1 10,000x	Invitrogen	S7563
TWEEN20	Sigma Aldrich	P9416
Critical commercial assays		
Tapestation 2200	Agilent Technologies	N/A
Novaseq S2 runs	Illumina	N/A
Nextera XT library preparation kit	Illumina	FC-131-1024
Deposited data		
RNA-seq and ATAC-seq data	Mendeley Data	https://doi.org/10.17632/cssc4vn6wv.1
Experimental models: Organisms/strains		
White leghorn chicken eggs	Charles River (MA)	N/A
Wild type mice (CD1)	Jackson Labs	N/A
Roslin GFP chick eggs	Clemson University	N/A
Budgerigar eggs	University of New Mexico	N/A
Gentoo penguin eggs	Weddell Island, Falkland Islands	N/A
Emu hatching eggs	Floeck's Country Farms	N/A
Ostrich hatching eggs	Floeck's Country Farms	N/A
Rhea hatching eggs	Floeck's Country Farms	N/A
memGFP quail eggs	University of Southern California	N/A
Alligator eggs	Rockefeller Wildlife Refuge	N/A
Oligonucleotides		
Barcode sequence 1 - Cy5 labeled barcode strand.	GGAGTTGGAGTGAGTGGATGAGTGATGDDDDDDDDDDDDTATGGATGAGTTATATAACTCA[cnvK]TCGTGTAAAT[Cy5-3]	Gene link
Barcode sequence 2 - Cy3 labeled barcode strand.	GGAGTTGGAGTGAGTGGATGAGTGATGDDDDDDDDDDDDGTTAGGTGAGTTATATAACTCA[cnvK]TCGTGTAAAT[Cy3-3]	Gene link
Barcode sequence 3 - Fluorescein (FITC) labeled barcode strand.	GGAGTTGGAGTGAGTGGATGAGTGATGDDDDDDDDDDDDAGGGTATGAGTTATATAACTCA[cnvK]TCGTGTAAAT[Fl-3]	Gene link
RT.5N.3G	TTTACACGATTGAGTTATNNNNNGGG	IDT
GATC.20T	GAGAATGTGAGTGAAGATGTATGGTGATTTTTTTTTTTTTTTTTTT	IDT
GATE	GGAGTTGGAGTGAGTGGATGAGTGATG	IDT
GATC	GAGAATGTGAGTGAAGATGTATGGTGA	IDT
P5.GATE	CGCCGGAGTTGGAGTGAGTGGATGAGTGATG	IDT
GATE*.P5*	CATCACTCATCCACTCACTCCAACTCCGGCG	IDT
CRABPI_chick_F	ttataaaagcttgcggccgcACATCAAAACTTCCACCACTGTCC	IDT
CRABPI_chick_R	gctctagaaattaaccctcactaaaggACACACACGGTCACATACAACACC	IDT
Cyp26c1_chick_F	ttataaaagcttgcggccgcCCACAAACCTGTGGTGAATAAATG	IDT
Cyp26c1_chick_R	gctctagaaattaaccctcactaaaggAAGGTCAGGAGGGGCAGAGG	IDT

(*Continued on next page*)

Please cite this article in press as: Longtine et al., Homology and the evolution of vocal folds in the novel avian voice box, Current Biology (2023), https://doi.org/10.1016/j.cub.2023.12.013

Continued

REAGENT or RESOURCE	SOURCE	IDENTIFIER
Aldh1a2_chick_F	ttataaaagcttgcggccgcGGTGCAGCAATAGC ATCTCA	IDT
Aldh1a2_chick_R	gctctagaaattaaccctcactaaaggTGAACAGGCCC AAAAATCTC	IDT
Aldh1a3_chick_F	ttataaaagcttgcggccgcCAACGGTGCTGTGGAGAAC	IDT
Aldh1a3_chick_R	gctctagaaattaaccctcactaaaggTAGGCCTCCTGT TTTCATGG	IDT
Rarres1_chick_F	ttataaaagcttgcggccgcAAGTCTCCGCCTGTAGTCCA	IDT
Rarres1_chick_R	gctctagaaattaaccctcactaaaggTTCATGAGACGTTC CAGCAG	IDT
Aldh1a2_paleognath_F	ttataaaagcttgcggccgcGGGAAGCTGATCCAAGAAGC	IDT
Aldh1a2_paleognath_R	gctctagaaattaaccctcactaaaggGCCAGACATTTTGA ATCCTCC	IDT
Aldh1a3_paleognath_F	ttataaaagcttgcggccgcGCCGTGGAGAACGGGCAGCC	IDT
Aldh1a3_paleognath_R	gctctagaaattaaccctcactaaaggGTGGGGCCATAGC CTGGCAC	IDT
Aldh1a2_mouse_F	ttataaaagcttgcggccgcGGCTGGGCTGATAAAATTCA	IDT
Aldh1a2_mouse_R	gctctagaaattaaccctcactaaaggTCTGAGGACCCTGC TCAGTT	IDT
Aldh1a3_gator_F	ttataaaagcttgcggccgcGCGTGTGTGGACAGATCATCCC	IDT
Aldh1a3_gator_R	gctctagaaattaaccctcactaaaggCCTGGTGAGCTTGTT CCACAGC	IDT
Aldh1a2_budgie_F	ttataaaagcttgcggccgcATTATGCTGGTTGGGCAGAC	IDT
Aldh1a2_Budgie_R	gctctagaaattaaccctcactaaaggCCCCACATTCAA GTTTTGCT	IDT
Software and algorithms		
STAR	https://github.com/alexdobin/STAR	N/A
Diffbind	https://doi.org/10.18129/B9.bioc.DiffBind	N/A
chromVar	https://github.com/GreenleafLab/chromVAR	N/A
DESeq2	https://doi.org/10.18129/B9.bioc.DESeq2	N/A
ImageJ	https://imagej.nih.gov/ij/	N/A
NGmerge	https://github.com/harvardinformatics/ NGmerge	N/A
Lightseq	https://github.com/Harvard-MolSys-Lab/Light-Seq-Nature-Methods-2022	N/A
Bedtools2	https://bedtools.readthedocs.io/en/latest/	N/A

RESOURCE AVAILABILITY

Lead contact

Further information and requests for resources and reagents should be directed to and will be fulfilled by the lead contact, Clifford J. Tabin (tabin@genetics.med.harvard.edu)

Materials availability

This study did not generate new unique reagents.

Data and code availability

- RNA-sequencing and ATAC-sequencing data as well as datasets for chromVar analysis of the ATAC-seq data have been deposited in Mendeley Data:https://doi.org/10.17632/cssc4vn6wv.1. Microscopy data reported in this paper will be shared by the lead contact upon request.
- This paper uses published analysis pipelines with modifications as described in the STAR Methods section.
- Any additional information required to reanalyze the data reported in this paper is available from the lead contact upon request.

Please cite this article in press as: Longtine et al., Homology and the evolution of vocal folds in the novel avian voice box, Current Biology (2023), https://doi.org/10.1016/j.cub.2023.12.013

EXPERIMENTAL MODEL AND STUDY PARTICIPANT DETAILS

Chicken

White leghorn chicken embryos were obtained from Charles River (MA) and incubated at 38°C.

Mouse

Timed-pregnant CD1 female mice were purchased from Charles River Laboratories.

Other animal species

- Ostrich, emu, and rhea embryos were obtained from Floeck's Country Farms (Tucumcari, NM) and incubated at 35°C until they reached appropriate stages.
- Roslin GFP chick eggs were obtained from Susan Chapman at Clemson University and memGFP quail eggs were obtained from Rusty Lansford at the University of Southern California
- Budgerigar embryos were obtained from Tim Wright and Angela Medina Garcia at the University of New Mexico
- Gentoo penguin embryos were collected from Weddell Island in the Western Falkland Islands (Research Licence No: R29/2022).
- Alligator embryos were obtained from Ruth Elsey at the Rockefeller Wildlife Refuge in Grand Chenier, Louisiana.
- Macaque larynx was a third trimester embryo of *Macaca mulatta* obtained as a formaldehyde-fixed dissected airway from the Oregon National Primate Research Center Tissue Distribution Program
- All embryos were collected in accordance with the appropriate Institutional Animal Care and Use Committee (IACUC) guidelines.

METHOD DETAILS

Tissue sample collection

White leghorn chicken embryos were obtained from Charles River (MA) and ostrich, emu, and rhea embryos were obtained from Floeck's Country Farms (Tucumcari, NM). Roslin GFP chick eggs[50] were obtained from Susan Chapman at Clemson University and memGFP quail eggs[51] were obtained from Rusty Lansford at the University of Southern California. Budgerigar embryos were obtained from Tim Wright and Angela Medina Garcia at the University of New Mexico, and Gentoo penguin embryos were collected from Weddell Island in the Western Falkland Islands (Research Licence No: R29/2022). Alligator embryos were obtained from Ruth Elsey at the Rockefeller Wildlife Refuge in Grand Chenier, Louisiana. Emus were staged according to Nagai et al.,[52] finches were staged according to Murray et al.,[53] and staging of all other avian embryos was carried out according to HH staging series.[18] Alligators were staged according to Ferguson[54] and incubated in moist vermiculite at 30°C. Chicken, duck, and budgerigar embryos were incubated at 38°C and ostrich, rhea, and emu embryos were incubated at 35°C until they reached appropriate stages. Timed-pregnant CD1 female mice were purchased from Charles River Laboratories. Macaque larynx was a third trimester embryo of *Macaca mulatta* obtained as a formaldehyde-fixed dissected airway from the Oregon National Primate Research Center Tissue Distribution Program. For all *in situ* hybridization, immunofluorescence, and histology experiments presented, images are representative of multiple sections from > 2 syrinxes (> 3 syrinxes for chick experiments).

Embryonic tissue was dissected in cold PBS and either directly processed for explant or cell culture or fixed in 4% formaldehyde and processed for cryo-embedding. Transplants were carried out using fine watchmaker's forceps and flame polished tungsten needles. Neural crest tissue was excised using tungsten needles and removed *in ovo* from a windowed non-GFP embryo. Neural crest tissue from the same axial level of a stage-matched GFP chick embryo was dissected in PBS with Penicillin/Streptomycin and inserted into the region of excised neural crest in the host embryo. Host embryos were then covered with PBS with Penicillin/Streptomycin, taped (Crystal Clear Gorilla Tape), and allowed to continue development. Neural crest electroporations were performed by injecting LiOn-CAG ∞ RFP and pCMV-hyPBase at 2 μg/μl final concentration with Fast Green dye into the neural tube using a mouth pipette and a pulled glass capillary needle at HH8 (n = 21), HH9 (n = 16), HH10 (n = 13), HH11 (n = 11), and electroporating laterally using 5 square pulses of 18V for 50 msec each with a 100 msec interval. To fate map the lateral plate mesoderm, Lentivirus-GFP with Fast Green dye to label injection site was injected at HH11 anteriorly into the coelom between the splanchnic and somatic lateral plate mesoderm at approximately the level of the most posterior somite until the injection mix reached the anterior intestinal portal. Successful infections of the lateral plate mesoderm were determined by presence of GFP in the foregut mesenchyme.

Tissue and cell culture

Chick syrinx explants were cultured in DMEM containing 1% Pen/Strep and 10% chick embryo extract (U.S. Biological) and grown in a humidified 37°C incubator with 5% CO_2. To prevent collapse, airways were dissected whole from the larynx to the lungs and pinned to a 4% agarose bed with 0.1mm minutien pins (FST) in a 6-well dish. Airways were pinned at the larynx and each lung and maintained taut but not stretched, with the explant positioned at the air-media interface to allow gas exchange. For cell culture, mouse tracheas, chick tracheas, or vocal folds were dissected in ice cold PBS and digested with 1x Trypsin in EDTA Solution (Sigma-Aldrich) at 37°C

Please cite this article in press as: Longtine et al., Homology and the evolution of vocal folds in the novel avian voice box, Current Biology (2023), https://doi.org/10.1016/j.cub.2023.12.013

for 15 minutes, just long enough to allow digestion of non-cartilage mesenchyme, and filtered through 35mm nylon mesh filters to remove the undigested cartilage. Cells were plated 20K/well of 24-well dishes and submerged in DMEM with 1% Pen/Strep and 10% FBS. For RCAS-treated cultures, 1μl RCAS virus was added to the culture medium. Mouse cells were transfected using polyethylenimine (PEI) with a CAGGS-BFP reporter alone or with pWPXL-SOX9. pWPXL-SOX9 was a gift from Bob Weinberg (Addgene plasmid #36979).

In ovo treatments with pan-RAR inhibitor AGN193109 (Sigma-Aldrich) and THRA inhibitor NH-3 (Med Chem Express) were performed by removing the shell overlying the air cell, peeling back the membrane and pipetting the drug onto the albumin to a final *in ovo* concentration of 5 μM before adding several drops of PBS with Penicillin/Streptomycin and closing the hole with tape.

Immunohistochemistry and *in situ* hybridization

Fixed embryos were dehydrated in sucrose gradients and embedded in OCT (Tissue-Tek). Sectioning was performed on a Leica CM3000 cryostat. For immunohistochemistry, sections were incubated with primary antibodies in PBST (PBS/BSA 0.2%, Triton 0.1% / SDS 0.02%) overnight, washed 2×10 minutes in PBST, incubated for 1 hour with secondary antibodies washed 2×10 minutes in PBST, and counterstained with DAPI. Primary antibodies used were anti-SOX9 (Millipore), anti-phosphoH3S10 (Millipore), anti-Cleaved Caspase 3 (Cell Signaling), anti-Laminin (Sigma-Aldrich), biotinylated-HABP (EMD Millipore), anti-Elastin (EMD Chemicals), anti-Versican (ThermoFisher), anti-phosphoYAP (Abcam), THRA (ThermoFisher), PDGFRa (R&D Systems), SERPINH1 (ThermoFisher), PTER (ThermoFisher), OTX2 (ProteinTech), TBX20 (Novus Biologics), VEGFC (ProteinTech), β-catenin (Millipore) at 1:500 dilutions, anti-Col2a1 (Developmental Studies Hybridoma Bank II-II6B3) at 1:50 dilution, and Alexa Fluor 647 Phalloidin (Invitrogen) at 1:50 dilution.

In situ probes were generated using transcript-specific PCR primers with T7 sequences added to the reverse primer to synthesize anti-sense DIG-labeled RNA probes. Fixed airways for whole-mount ISH were stored at -20°C in methanol, graded into PBT (1x PBS/0.1% Tween-20), permeabilized with 10 μg/ml of proteinase K for 15 min, refixed in 4% formaldehyde and then hybridized overnight at 70°C. Unbound probe was washed out with SSC washes at 72°C and the embryos were then blocked in Blocking Reagent (Millipore) and incubated with anti-DIG-AP antibodies overnight (1:2000). Unbound antibodies were washed out with TBST (1x TBS/0.1% Tween-20) washes and probes were visualized BM purple (Sigma-Aldrich). Cryosectioned tissue for section *in situs* were fixed in 4% formaldehyde, permeabilized with 1 μg/mL proteinase K for 20 min, refixed in 4% formaldehyde and hybridized overnight at 60°C. Unbound probe was washed out with SSC washes and the embryos were then blocked in Blocking Reagent (Millipore) and incubated with anti-DIG-POD (1:300, Sigma-Aldrich). Unbound antibodies were washed out with TBST washes, and bound probe was visualized with Cy3 TSA amplification (Perkin Elmer). Fluorescent images were acquired on a Nikon Ti inverted microscope with a W1 Yokogawa Spinning disk using Plan Apo λ 20x/0.75 and Plan Fluor 40x/1.3 Oil objectives.

To quantify ECM deposition in RCAS-infected cell cultures, images were processed using a grid-based method in ImageJ. Fields of view were divided into randomly placed tiled grids approximately 5 cells wide, and mean intensity from each channel was quantified.[55] SOX9 and HA immunofluorescence intensity was quantified by manually segmenting vocal folds (the non-cartilage mesenchymal tissue between the 2 enlarged syringeal cartilage elements visualized using DAPI), and mean vocal fold fluorescence intensities for SOX9 and HA were compared using a Welch two-sample t-test in R.

Ancestral state reconstruction

We tested two models of discrete trait evolution with fitDiscrete in the geiger R package[56]: an equal rates (ER) model in which gains and losses of two sound sources occur at equal rates and an all rates different (ARD) model in which gains and losses are allowed to take on different rates. To account for phylogenetic uncertainty, we fit ER and ARD models to each of two recent time-calibrated bird phylogenies.[57,58] In each case, the ER model fit the data better than the ARD model (AIC weights for the ER model = 0.70 and 0.79 for the Prum et al. and Kimball et al. phylogenies, respectively), thus we used this simpler ER model for subsequent ancestral state reconstructions.

Ancestral state reconstruction under the ER model showed strong support for paired sound sources at the root (P = 0.99). To assess the robustness of this result to uncertainty in species scorings, we inverted ambiguous species' scores (i.e., from single to paired sound sources, or vice versa) and re-estimated ancestral states at the root under the ER model to determine the species score influence. Uncertainty in scoring for ostrich has little effect on root state (Figure S5C).

To further assess the influence of incomplete taxon sampling on the root ancestral state, we used a large phylogeny[59] with branch lengths from Riede et al.[60] We then simulated 100 evolutionary histories using stochastic character mapping in make.simmap, with a fixed transition rate (estimated from the ER model using 14 species with known values) and uncertain species (n = 6698) coded as ambiguous. The estimated evolutionary rate is likely an overestimate of the true rate, as further sampling of species (e.g., within passerines) would likely reduce the rate and further improve support for paired sound sources in the ancestor of Aves (at high rates, the probability expectedly approaches 0.5).[61] Ancestral states were then summarized along simulated histories with the describe.simmap function in phytools.[62] Ancestral state reconstruction for the presence of pessulus and intrinsic syringeal musculature was also performed using the phytools package in R using the make.simmap function in to generate 1000 stochastic character maps, which we then used to plot the probability densities using the densityMap function on a recent time-calibrated phylogenetic tree inferred from genomic data.[58] We scored the ostrich as lacking a pessulus, although a non-ossified pessuliform process has been reported in ostrich[63,64] (the presence of a pessulus in ostrich increases the probability of a pessulus at the root of Aves from 0.64 to 0.90).

Please cite this article in press as: Longtine et al., Homology and the evolution of vocal folds in the novel avian voice box, Current Biology (2023), https://doi.org/10.1016/j.cub.2023.12.013

Syrinx endoscopy

To view the movement of vocal tissues in the chicken syrinx, we anaesthetized four 8-day-old chicks with isoflurane and applied local anesthetic to the skin (Cetacaine) before exposing the trachea in the neck area. We then applied Cetacaine to the tracheal surface and made an incision in the trachea approximately 2 cm above the tracheobronchial junction. We inserted an angiofiberscope (Hawkeye Precision Boreoscope, 0.9 mm diameter) into the trachea, guided the lens toward the syrinx, and recorded video at 30 frames per second during normal respiration and spontaneous phonation. All experiments were in accordance with the IACUC of the University of Utah, Salt Lake City, USA.

MicroCT scanning

Syrinxes from juvenile and adult bird specimens (*Struthio camelus* – 2-day-old: TMM-14733, 14-day-old: TMM-14777, adult male: TMM-14723, adult female: TMM-15832, *Dromaius novaehollandiae* – juvenile: TMM-13032, adult male: YPM 139717, and *Gallus gallus* – 2-day-old: UMNH-23840, adult female: UMNH-23828) were imaged using iodine-enhanced contrast x-ray computed tomography. After being preserved in 70% EtOH, specimens were stained in 3.75% I2E (w/v) in 100% EtOH solution. Stained specimens were then scanned in a custom NSI helical scanner at UTCT at the University of Texas at Austin, producing stacks of 16-bit tiffs. For juvenile Ostrich specimens, we used a peak voltage of 150 kV, current of 0.2 mA, and a voxel size of 25.4 μm with no filter. For the adult female Ostrich, we used a peak voltage of 150 kV, current of 0.24 mA, and a voxel size of 30.4 μm with an aluminum filter, and for the adult male, peak voltage of 140 kV, current of 0.15 mA, and a voxel size of 102.2 μm with an aluminum filter. For the juvenile emu, we used a peak voltage of 120 kV, current of 0.15 mA, and a voxel size of 46.0 μm. For the adult emu, we used a peak voltage of 140 kV, current of 0.21 mA, and a voxel size of 94.7 μm. For the adult domestic chicken, we used a peak voltage of 160 kV, current of 0.21 mA, and a voxel size of 27.2 μm. Specimens were segmented and 3D visualizations were created using the volume rendering and surface view functions in Avizo.

RCAS

RCAS-BP(A) viral plasmid containing mScarlet, chicken SOX9, or a dominant-negative truncation of SOX9[25] were used to generate concentrated viral supernatant as described previously.[65]

Light-seq RNA sequencing

Chick and mouse airways were dissected in 1x PBS and immediately fixed for 1 hour at room temperature in 1x PBS with 4% formaldehyde, washed in 1x PBS, and graded through 7% sucrose into a 1:1 solution of OCT (Tissue-Tek) and 30% sucrose in 1x PBS for freezing and cryosectioning at into 20-μm sections on poly-L-lysine coated Ibidi chamber slides. To promote tissue adhesion, slides were centrifuged at 800 rcf for 5 minutes. *In situ* RT and A-tailing, barcoding, cross-junction synthesis, displacement, and library preparation was performed as described previously[20] with the following modifications. We used 2 mg/ml sheared salmon sperm DNA (invitrogen) and 10% dextran sulfate in the barcode hybridization mix to reduce non-specific barcode binding. During the displacement step, we pipetted the RNase H containing solution up and down several times every 15 minutes during the 45-minute incubation at 37°C to increase yield of recovery. Samples were tagmented with a Nextera XT library preparation kit (Illumina) using custom primers for the i5 end as previously described.[20] Sequencing was performed on a NextSeq500 with a read length of 150 and 30% PhiX spike-in. All replicates were pooled together and sequenced across two lanes of a NextSeq500 run.

Sequencing data analysis was performed using published Light-seq analysis code[20] on the Harvard Medical School O2 cluster (Kernel 2.10.0) with Python (v3.7.5), PyTable (v3.6.1), samtools (v1.12), pysam (v0.17.0), numpy (v1.21.4), pandas (v1.3.4), Biopython (v1.79), and scikit-bio (v0.5.6). Briefly, Barcode, UMI, and cDNA sequences were extracted from Read 1 using UMI-tools (v1.1.1). cDNA sequence was then mapped to either the chick (GG6a) or mouse (M27) genomes. Reads were assigned to genes using FeatureCounts using fractional read counting and the GTF annotation 'gene' (-M –fraction -g gene_id -t gene) and deduplicated (per gene) with UMI-tools dedup.[66] Reads were parsed out by barcode sequences using a custom python script.[20] Differential gene expression analysis was performed in R (v3.6.1) using DESeq2.[67] Volcano plots were produced using ggplot2 (v3.4.0), and enriched genes and k-means clustering were plotted using the pheatmap function (v1.0.12).

ATAC-seq

ATAC-seq was performed using standard protocols.[21] Single-cell suspensions of HH39 chick vocal folds and HH34 trachea and tracheobronchial junction were prepared by dissecting the tissue in ice cold 1x PBS and digesting the tissue in 1x Trypsin in EDTA Solution (Sigma-Aldrich) at 37°C for 15 minutes with constant pipetting. Cell suspensions were filtered through 35mm nylon mesh filters, pelleted at 200 rcf for 5 minutes, washed in PBS with 1% BSA, pelleted again at 200 rcf for 5 minutes, then resuspended in 50–100μl PBS with 1% BSA. After processing 50,000 cells per sample using the standard Omni-ATAC protocol,[21] samples were pooled and run on Tapestation 2200 (Agilent Technologies) to assess library quality. Four biological replicates were performed for each tissue type. Samples were pooled and sequenced on two Novaseq S2 runs (Bauer sequencing core, Harvard University) to a depth of at least 50M reads per sample. Demultiplexed reads were trimmed of adapter sequences using NGmerge (v0.3) and aligned to the chick genome (GG6a) using Bowtie2 (v2.5.1). Peaks were called for each replicate and a consensus peak set with a fixed center and standardized width of 200 bps was created using Genrich for input into chromVAR.[22] For chromVAR analysis, we followed the default walkthrough (https://greenleaflab.github.io/chromVAR/articles/Introduction.html) using the galGal6 BSgenome package and the human_pwms_v1 position weight matrices to identify transcription factor binding sites using the matchMotifs

Please cite this article in press as: Longtine et al., Homology and the evolution of vocal folds in the novel avian voice box, Current Biology (2023), https://doi.org/10.1016/j.cub.2023.12.013

command in the motifmatchr R package (v1.2.0). Peaks from the scaffold "chrUn_NW_020109859v1" were removed prior to correcting for GC bias and computing motif variability, as it does not appear in the galGal6 BSGenome file. The nearest transcriptional start site (TSS) to each peak was calculated using Bedtools (v2.27.1).

Network inference

To infer putative gene regulatory networks in the chick trachea and vocal folds, we first constructed a base network containing unweighted, directional edges between TFs and their target genes. We assigned TF binding motifs in regions of open chromatin to the nearest TSS as described above to narrow the scope of potential regulatory interactions between tissue-specific genes. This base network likely contains many inactive connections, so we calculated normalized mutual information between gene pairs to determine the co-dependence of gene expression between transcription factors and their putative targets. Normalized mutual information (NMI) was calculated as:

$$\mathrm{NMI}\ (X, Y)\ =\ 2I(X, Y)H(X) * H(Y)$$

Where *I(X,Y)* is the mutual information between gene expression count vectors of genes X and Y in all samples and *H(X)* and *H(Y)* are the entropy of gene expression count vectors of genes X and Y. We next constructed a total network in which nodes represent TFs with detectable gene expression in our Light-seq data and edges represent connections determined by presence of transcription factor binding sites and an NMI $\geq$ 0.8. To visualize tissue-specific putative regulatory networks, we built networks using only transcription factors which were significantly more accessible in either vocal fold or tracheal ATAC-seq data (determined using chromVAR as above). To determine local connectivity of these tissue-specific networks, we subsampled networks from the tissue-specific network and the total network and calculated the density (the proportion of possible connections which are present in the graph). Both the VF and the tracheal networks are significantly more locally connected than random subsets of the same size ($P < 0.001$, Welch 2-sample t-test). Eigenvector centrality, density, and degree were calculated in R using the package iGraph (v1.4.1). Mutual information and entropy were calculated in R using the package infotheo (v1.2.0.1).

QUANTIFICATION AND STATISTICAL ANALYSIS

For all *in situ* hybridization, immunofluorescence, and histology experiments presented, images are representative of multiple sections from > 2 syrinxes (> 3 syrinxes for chick experiments). To quantify ECM deposition in RCAS-infected cell cultures (Figures 3C, 3D, 6D, and S3D), images were processed using a grid-based method in ImageJ. Fields of view were divided into randomly placed tiled grids approximately 5 cells wide, and mean intensity from each channel was quantified.[55] SOX9 and HA immunofluorescence intensity was quantified by manually segmenting vocal folds (the non-cartilage mesenchymal tissue between the 2 enlarged syringeal cartilage elements visualized using DAPI), and mean vocal fold fluorescence intensities for SOX9 and HA were compared using a Welch two-sample t-test in R. For details on ancestral state reconstructions, see sections above (Method details, ancestral state reconstruction). For ATAC-sequencing, differentially accessible peaks were calculated using Diffbind, and variable TF binding sites were calculated using chromVAR. t-SNE was performed in chromVAR using biased-corrected deviations with threshold = 1.5, perplexity = 5 (Figure 2H). Differentially expressed genes in Lightseq datasets were calculated using DESeq2 using padj < 0.01 and log2FoldChange > 2.